

Magnetospheric effects on high-energy solar particles during the 2012 May 17th event measured with the PAMELA experiment

M. Martucci^{1,2}, G. A. Bazilevskaya³, M. Boezio⁴, U. Bravar⁵, A. Bruno⁶, E. R. Christian⁷, G. A. de Nolfo⁷, M. Lee⁵, M. Merge^{1,8}, E. Mocchiutti⁴, R. Munini^{4,9}, M. Ricci², J. M. Ryan⁵, S. Stochaj¹⁰, N. Thakur⁷, O. Adriani^{11,12}, G. C. Barbarino^{13,14}, R. Bellotti^{6,16}, E. A. Bogomolov¹⁷, M. Bongj^{11,12}, V. Bonvicini⁴, S. Bottai¹², F. Cafagna¹⁶, D. Campana¹⁴, P. Carlson¹⁹, M. Casolino^{8,20}, G. Castellini²¹, C. De Donato^{1,8}, C. De Santis⁸, N. De Simone⁸, V. Di Felice^{8,24}, V. Formato^{4,9,x}, A. M. Galper¹⁸, A. V. Karelin¹⁸, S. V. Koldashov¹⁸, S. Koldobskiy¹⁸, S. Y. Krutkov¹⁷, A. N. Kvashnin⁵, A. Leonov¹⁸, V. Malakhov¹⁸, L. Marcelli¹, A. G. Mayorov¹⁸, W. Menn²², V. V. Mikhailov¹⁸, A. Monaco^{6,16}, N. Morj^{12,25}, G. Osteria¹⁴, F. Palma^{1,8}, B. Panico¹⁴, P. Papini¹², M. Pearce¹⁹, P. Picozza^{1,8}, S. B. Ricciarini^{12,21}, R. Sarkar^{4,**}, V. Scotti^{13,14}, M. Simon²², R. Sparvoli^{1,8}, P. Spillantini^{11,12}, Y. I. Stozhkov⁵, A. Vacchi⁴, E. Vannuccini¹², G. Vasilyev¹⁷, S. A. Voronov¹⁸, Y. T. Yurkin¹⁸, G. Zampa⁴ and N. Zampa⁴

¹ Department of Physics, University of Rome "Tor Vergata" I-00133 Rome, Italy

² INFN, Laboratori Nazionali di Frascati, Via Enrico Fermi 40, I-00044 Frascati, Italy

³ Lebedev Physical Institute, RU-119991 Moscow, Russia

⁴ INFN, Sezione di Trieste, I-34149 Trieste, Italy

⁵ Space Science Center, University of New Hampshire, Durham, NH, USA

⁶ University of Bari, I-70126 Bari, Italy

⁷ Heliophysics Division, NASA Goddard Space Flight Center, Greenbelt, MD, USA

⁸ INFN, Sezione di Rome "Tor Vergata", I-00133 Rome, Italy

⁹ University of Trieste, Department of Physics, I-34147 Trieste, Italy

¹⁰ Electrical and Computer Engineering, New Mexico State University, Las Cruces, NM, USA

¹¹ University of Florence, Department of Physics, I-50019 Sesto Fiorentino, Florence, Italy

¹² INFN, Sezione di Florence, I-50019 Sesto Fiorentino, Florence, Italy

¹³ University of Naples "Federico II", Department of Physics, I-80126 Naples, Italy

¹⁴ INFN, Sezione di Naples, I-80126 Naples, Italy

¹⁵ Lebedev Physical Institute, RU-119991, Moscow, Russia

¹⁶ INFN, Sezione di Bari, I-70126 Bari, Italy

¹⁷ Ioffe Physical Technical Institute, RU-194021 St. Petersburg, Russia

¹⁸ National Research Nuclear University MEPhI, RU-115409, Moscow, Russia

¹⁹ KTH, Department of Physics, and the Oskar Klein Centre for Cosmoparticle Physics, AlbaNova University Centre, SE-10691 Stockholm, Sweden

²⁰ RIKEN, Advanced Science Institute, Wako-shi, Saitama, Japan

²¹ IFAC, I-50019 Sesto Fiorentino, Florence, Italy

²² Universität Siegen, Department of Physics, D-57068 Siegen, Germany

²⁴ Agenzia Spaziale Italiana (ASI) Science Data Center, I-00044 Frascati, Italy

²⁵ Centro Siciliano di Fisica Nucleare e Struttura della Materia (CSFNMSM), Viale A. Doria 6, I-95125 Catania, Italy

^x now at INFN, Sezione di Perugia, I-06123 Perugia, Italy

^{**} now at Indian Centre for Space Physics, 43 Chalanika, Garia Station Road, Kolkata 700084, West Bengal, India

E-mail: matteo.martucci@roma2.infn.it

The great challenge in constraining scenarios for solar energetic particle (SEP) acceleration is due to the fact that the signatures of acceleration itself are heavily modified by transport within interplanetary space. During transport, SEPs are subject to pitch angle scattering by the turbulent magnetic field, adiabatic focusing, or reflecting magnetic structures. Ground Level Enhancements (GLEs) provide an ideal way to study acceleration with minimal transport. In this work, we present a unique high-energy SEP observation from PAMELA of the 2012 May 17 GLE and interpret the observed pitch angle distributions as a result of local scattering (1 AU) by the Earth's magnetosheath.

*The 34th International Cosmic Ray Conference,
30 July- 6 August, 2015
The Hague, The Netherlands*

*Speaker.

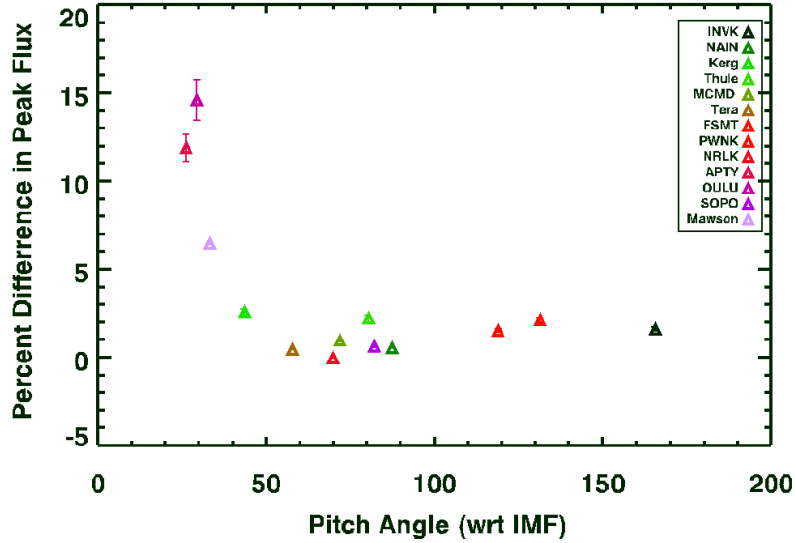


Figure 1: Neutron Monitor percentage flux as a function of pitch angle, averaged between 0158 and 0220 UT.

1. Introduction

The Sun could accelerate particles at low altitudes through magnetic reconnection or higher in the corona through coronal mass ejection-driven (CME) shocks, but the scenario is still uncertain. This uncertainty exists at the very lowest energies of Solar Energetic Particles (SEPs) observed in situ and also persists through Ground Level Enhancements (GLEs). Moreover, besides confounding the study of particle acceleration, the physics of energetic particle transport within the heliosphere is its own topic of study. The highest energy SEPs (observed in GLEs) provide an idealized case study in that the effects of transport are often minimal, even if the mechanisms of transport at lower energies is still poorly understood. The unique observations from the Payload for Antimatter Matter Exploration and Light-nuclei Astrophysics (PAMELA) instrument, provide an essential link between the highest-energy GLEs and the low-energy direct observations within the inner heliosphere.

2. The 2012 May 17th GLE

PAMELA observed the first GLE of solar cycle 24 (the number 71 overall), that took place on May 17th of 2012. Significant count rates ($\geq 15\%$ over background) were first registered by the Apatity neutron monitor (NM) at 0150 UT [Papaioannou 2014]. NMs at Oulu and Mawson also registered the event with signals $\sim 15\%$ over the background [Adriani 2015]. All three NMs had viewing angles close to the interplanetary magnetic field (IMF) direction [Mishev 2013, Papaioannou 2014]. The South Pole and Polar Bare NMs also registered a prompt signal despite having viewing directions far from the IMF, as well as ICETop [Kuwabara 2013]. This prompt signal was followed by a broader one, registered in all of the above NMs but also in other stations even if at a few-percent level. This is shown in Fig 1.

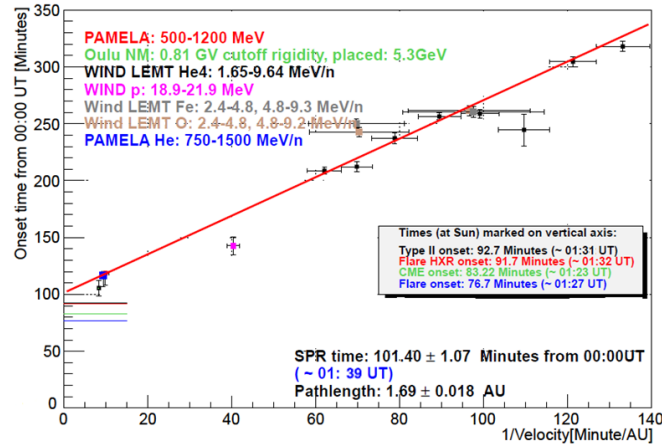


Figure 2: Onset time as a function of the velocity dispersion for the May 17th event, obtained by combining data sets from various instruments. The horizontal marks indicate the onset of the flare, CME-driven shock, type-II radio emission and hard X-ray component.

The GLE was associated with an M5.1 flare in active region AR 11476 located on the western limb of the Sun (N07W88). SOHO/LASCO measured an associated fast CME with a maximum speed of 1997 km [Gopalswamy 2013]. Type II radio emission was also reported by Solar Geophysical Data at 0131 UT which means that a shock took place. The computed injection time (delayed by eight minutes from the formation of the shock, 0131 UT) at the Sun using NM data, plus WIND He data and an upper limit from PAMELA was found to be 0139 ± 1 UT [Thakur 2012], like it can be seen in Fig 2.

The presence of accelerated high-energy ions at the Sun is inferred by the >100 MeV γ -ray emission [Ajello 2014]. However, even at GLE energies (>1 GeV), an evolving pitch angle distribution results from transport effects that are complex and which complicate the interpretation of the data [Adriani 2015]. GLEs often consist of a fast onset (and anisotropic) associated with a beam of field-aligned particles, which has been interpreted as a result of magnetic focusing. As the event progresses and the particle diffuse inside the heliosphere, the distribution becomes isotropic due to a process of scattering. This isotropic component is a result of scattering off a magnetic structure beyond Earth, or maybe to a magnetic bottleneck [Bieber 2002]. The shape and morphology of GLEs is usually determined through modelling of the response of the network of NMs located at differing regions of the planet. While there has been success in modelling some features of the incoming GLE beam, this method depends on the NM yield function and the assumption of vertical asymptotic directions. Moreover, their count rate is linked to the particle intensity integrated over a wide solid angle and with energies above a fixed geomagnetic cutoff [Adriani 2015]. For this reason, to fully understand the anisotropy evolution, measurements over a broad range in energy are required, and also the ability to determine directly the pitch angle at energies above 1 GeV, corresponding to the energy range of high-latitude NMs.

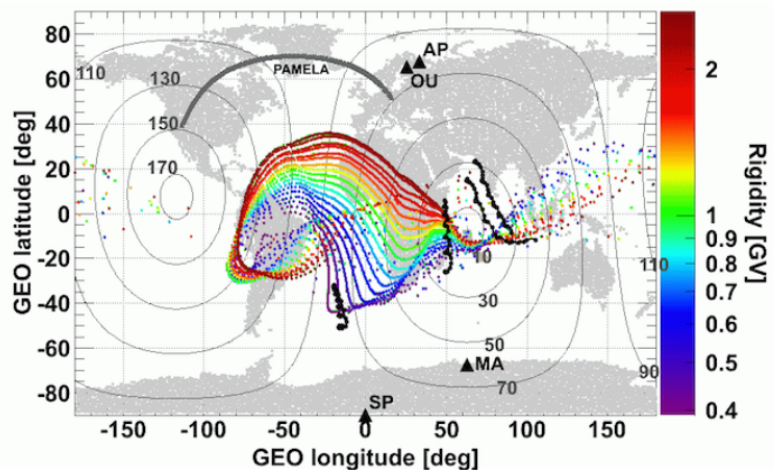


Figure 3: Asymptotic directions determined during the first polar pass that registered the event. Also shown are the asymptotic directions of the NM that registered the primary GLE beam. OU, AP, SP, and MA stand for Oulu, Apatity, South Pole, and Mawson NMs, respectively.

3. PAMELA observations

Details of the instrument structure, performance, particle selection, and selection efficiencies can be found in [Adriani 2013]. PAMELA measures the incident trajectory of the detected particles employing a combination of trajectory reconstruction with the silicon tracking system and particle tracing techniques. Its field of view is narrow ($\sim 20^\circ$). Because it is a moving platform, it sweeps through pitch angle space allowing one to construct a pitch angle distribution of the SEPs. For this study, we employed the particle tracing techniques of [Smart 2000] to determine the asymptotic direction for each incident particle with respect to the IMF. An explanation of our tracing techniques, which is based on an internal field model IGRF-2011 [Finlay 2010] and on an external field model TS-07 [Tsyganenko 2007] can be found in [Bruno 2014]. Solar wind and IMF parameters were obtained from the high-resolution Omniweb database (omniweb.gsfc.nasa.gov). While NMs measure the particle intensity for a given pitch angle (above the local cutoff rigidity), PAMELA is a moving observatory with a sensitivity to both energy and a pitch angle that depends on spacecraft location [Adriani 2015].

4. Results

Fig 3 shows the computed asymptotic vertical direction for PAMELA during the polar pass that first registered the 2012 May 17 event. Colour coding reflects the particle rigidity ranging from 0.4 to 2.4 GV. The grey solid curve shows the spacecraft trajectory for periods when PAMELA is at geomagnetic locations where the Störmer vertical cutoff is lower than 390 MV (Störmer 1950; Smart et al. 1965). The direction of the IMF obtained from the Omniweb database is shown as the black cross. Contours of constant pitch angle relative to the direction of the IMF are also shown.

As noted above, PAMELA is sensitive to a small range in pitch angle distribution that varies along the orbit and samples its distribution distribution from 0° to about 140° during the 20 minute polar pass. Fig 4 (top panel) shows the particle intensity (corrected for background) in two rigidity

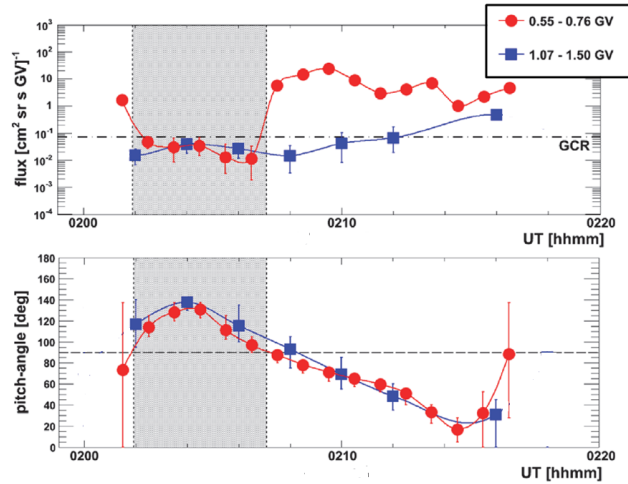


Figure 4: (top) Flux of SEPs registered by PAMELA in two different rigidity ranges. (bottom) Mean pitch angle distribution as a function of time during the polar pass under study. The dashed line represents the 90° pitch angle, while the shaded grey area represents the time during which PAMELA is above 90° of pitch angle. GCR background (calculated two days before the event itself) is indicated as a dashed line. The curves through the data are meant to guide the eye.

ranges observed by PAMELA. On the other hand, in the bottom panel, the pitch-angle distribution for which PAMELA is sensitive as a function of time is depicted.

The intensity was computed as a function of pitch angle and rigidity by correcting registered proton counts for the instrument efficiencies, livetime, and gathering power of the instrument at each orbital position, taking into account the anisotropic flux exposition and the change in look directions [Bruno 2014]. The background intensity (black dashed curve), due to galactic cosmic rays (GCRs), was estimated using data registered two days prior to the event. Within a given pitch angle distribution, the GCR background is isotropic, as expected. Comparing this top panel with the bottom panel, we can see how the proton fluxes varied as a function of pitch angle (and thus time). During times when PAMELA is sensitive to pitch angles $<90^\circ$, we observe an increase in the flux of 0.55-0.76 GV particles. Furthermore, when PAMELA is beyond 90° (shaded region), we see the 0.55-0.76 GV particle return to the background, reflecting the passage of PAMELA into and out of a low-energy component confined to the forward pitch-angle hemisphere. At high rigidities (>1 GV) the flux is constant for pitch angles greater than 40° , and increases markedly at small angles (note the logarithmic scale). PAMELA observed the event ~ 10 minutes after the Apatity onset (0150 UT) and continued to observe the event during the rising phase of the prompt emission as viewed by Apatity, Oulu, Mawson, and south pole. The dependence on pitch angle for three different energy regimes is shown in Fig 5.

PAMELA observes two populations simultaneously with very different pitch angle distributions. We see a low-energy component (0.39-1.07 GV) confined to pitch angles $<90^\circ$ and a high-energy component (1.50-2.09 GV) that is beamed with pitch angles $<30^\circ$, consistent with NM observations (Fig 5). The component with intermediate energies (1.07-1.50 GV) suggests a transition between the low and high energies, exhibiting a peak at small pitch angles and a cutoff at 90° .

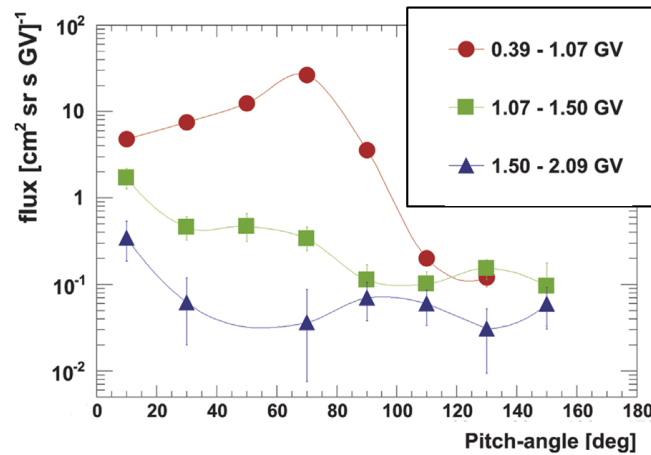


Figure 5: PAMELA's pitch angle distribution (background subtracted) in 3 rigidity ranges. The curves through the data are meant to guide the eye.

At rigidities >1 GV, corresponding to NM data, the particles are mostly field aligned. Assuming symmetry about the IMF, this would suggest a beam full width of $\sim 40\text{-}60^\circ$. Given the nature of the PAMELA observations, it is difficult to understand if or how these populations evolve during the ~ 20 minutes polar pass, however, it is striking that two distinct populations are present simultaneously relatively soon after the onset of the event as registered by the NMs. A complete discussion on this topic can be found in [Adriani 2015].

5. Discussion

GLEs typically become isotropic with time; however, this is the first time that a GLE has been observed, shortly after the onset, where the anisotropic component is accompanied by a broader enhancement that has presumably undergone significant scattering. We believe that the scattering responsible for the broader distribution at lower rigidities must take place locally as implied by the time coincidence of the highly scattered particles and the beamed particles. To better understand this, we note that the transit time for a zero-pitch-angle proton (which will travel over 1.2 AU) of rigidity 400 MV is ~ 1400 s. For a pitch angle of 60° the same proton would take 2800 s. This should be compared to the transit time for a 1 GV proton with a pitch angle of 20° (~ 890 s), a discrepancy of 1910 s. This is a lower limit to the discrepancy since the prevailing solar wind speed was slower than usual, ~ 365 km s^{-1} (translating to larger path lengths than the nominal 1.2 AU). For both populations to be present at Earth at the same time, they must have had similar transit times followed by local scattering to explain the presence of large pitch angle particles at low rigidity. The transit time for our original 400 MV proton at a pitch angle of 20° is ~ 1490 s—a discrepancy of less than 600 s. This difference for similar pitch angles is reasonable given the seven minute offset from the GLE onset. However, the low-rigidity particles at much greater pitch angles are not compatible with these numbers. Thus, these two pitch-angle distributions, narrow and broad, could not have co-existed at injection. The anisotropic nature of the >1 GV

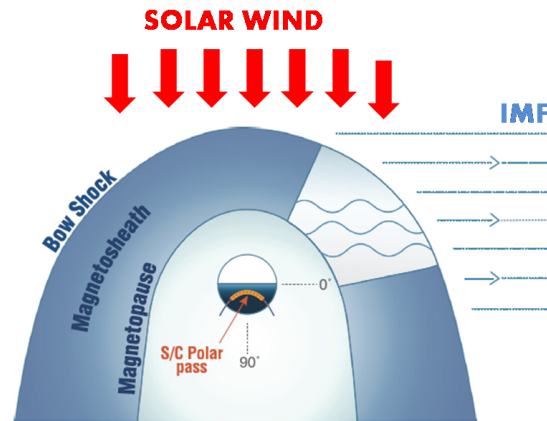


Figure 6: Particle transport for the May 17th GLE through the Earth's magnetosphere. Due to the quasi-perpendicular nature of the IMF, mirror mode fluctuations are enhanced that redistribute the low-energy SEPs preferentially. The polar orbit of PAMELA is shown for context.

particles was present for at least 30 minutes, starting from the onset (0150 UT), as registered with the NM network, through the 1 GV exposure times with PAMELA at 0220 UT. The scattered component was registered as early as 0157 UT on the leading edge of the well-connected NM signal representing an extended overlap in time of the two different populations. There are few candidate volumes or processes that are capable of producing the effect that are local. If we assume that the field-aligned distribution initially applied to a wide range of rigidities, covering the PAMELA range, then we must search for local agents that disperse or broaden that distribution preferentially at lower rigidities while leaving the higher-rigidity particles relatively unaffected. Three choices emerge as possibilities: (1) upstream turbulence in the solar wind in the form of Alfvén waves, (2) the intense and chaotic fields in the Earth's bow shock itself, and (3) the Earth's magnetosheath. The upstream rms magnetic field, a measure of the turbulence present, did not exceed 1 nT for several days after the event while the IMF ranged between 5 and 10 nT¹. so the first hypothesis appears to be not correct. The intense turbulence in the Earth's bow shock is probably insufficient to produce the effect given the thinness of the shock, of the order of 20 km [Schwartz 2011]. However, the magnetosheath possesses an intense magnetic field (≥ 20 nT) with typically large-amplitude mirror mode instability fluctuations ($\geq 50\%$) and is much thicker (several R_E [Southwood 1993]).

The diagram in Fig 6 schematically shows the orientation of the IMF, the bow shock, magnetosphere, the particle asymptotic directions, and the spacecraft trajectory of the PAMELA measurements. The IMF is mostly tangential to the solar wind ($B_y \gg B_x$ or $B-z$) with the high-rigidity particles entering the magnetosphere on the dawn-side flank. The lowest rigidity particles are detected near local midnight. On the dawn side flank the magnetosheath is much thicker, of the order of $5 R_E$ or greater. In this sheath the fluctuations are in the form of mirror mode, non-propagating waves. These convect down the flanks of the magnetosphere as quasi-static large-amplitude structures with a spatial scale in the plasma rest frame of 1000-2000 km [Gutynska 2008]. Depending

¹Farrugia priv. comm.

on the point of entry into the magnetosheath and the phase of the gyration about the mean field, equal rigidity, field-aligned particles would take different paths, effectively dispersing in pitch angle when they enter the quieter magnetosphere and the instrument orbit. Pitch angle diffusion, in the sense of scattering off Alfvén waves, would not be significant and the particles would continue on a forward path and not be scattered backward unless there was mirroring taking place-not possible at these rigidities. Smaller gyroradius (lower rigidity) particles would be more affected. Because the wave amplitude is comparable to the mean field, comparing the mean gyroradius to the magnetosheath thickness is a useful indicator of the magnitude of the effect one would expect. For example, a 400 MV proton in the ambient 20 nT field has a gyroradius of $\sim 12 R_E$, while a 1.5 GV proton has a gyroradius of $\sim 40 R_E$. These are encouraging numbers in that this would imply significant, but not too intense, dispersion in the $5 R_E$ thick magnetosheath for the 1.5 GV GLE protons, but much greater dispersion for the lower-rigidity particles.

The distorted orientation of the IMF may be a key factor in the anisotropy effect observed in the particle intensities because entry into the magnetosphere on the flank significantly increases the diffusive volume compared to the nominal 45° of the Archimedes spiral and because the quasi-perpendicular nature of the IMF is exactly what is needed to produce large mirror mode fluctuations. This is the first observation of differential dispersion as particles transit the magnetosheath. Low-energy solar energetic protons were registered within the Earth's magnetosheath [Debrunner 1984] that qualitatively show similar anisotropies to the high-energy. A complete discussion on this topic can be found in [Adriani 2015].

References

- [Adriani 2015] Adriani, O. *et al.*, *ApJL* **801** (2015) L3.
 [Papaioannou 2014] Papaioannou, A. *et al.*, *SoPh* **289** (2014) 423.
 [Mishev 2013] Mishev, A. L. *et al.*, *JGRA* **119** (2013) 670.
 [Kuwabara 2013] Kuwabara, T. *et al.*, *Proc. 33rd ICRC* (2013) submitted:arXiv:1309.7006.
 [Gopalswamy 2013] Gopalswamy, N. *et al.*, *ApJL*, **765** (2013) L30.
 [Thakur 2012] Thakur, N. *et al.*, in *2013 Spring Meeting (Washington, DC: AGU)*, Abstract SH21A-2186.
 [Ajello 2014] Ajello, M. *et al.*, *ApJ* **789** (2014) 20.
 [Bieber 2002] Bieber, J. W. *et al.*, *ApJ* **567** (2002) 622.
 [Picozza 2007] Picozza, P. *et al.*, *Aph* **27** (2007) 296.
 [Adriani 2013] Adriani, O. *et al.*, *ApJ* **765** (2013) 91.
 [Smart 2000] Smart, D. F. *et al.*, *SSRv* **93** (2000) 305.
 [Finlay 2010] Finlay, C. C. *et al.*, *GeoJI*, **183** (2010) 12161230.
 [Tsyganenko 2007] Tsyganenko, N. *et al.*, *JGR* **112** (2007) A06225.
 [Bruno 2014] Bruno, A. *et al.* (2014) submitted:arXiv:1412.1765.
 [Schwartz 2011] Schwartz, S. *et al.*, *PhRvL* **107** (2011) 215002.
 [Southwood 1993] Southwood, D. J. *et al.*, *JGR* **98** (1993) 9181.
 [Gutynska 2008] Gutynska, O. *et al.*, in *WDS08 Proc. Contributed Papers: Part II- Physics of Plasmas and Ionized Media*, ed. J. Safrankova, & J. Pavlu (Prague: Matfyz press) (2008) 151.
 [Debrunner 1984] Debrunner, H. *et al.*, *JGR* **89** (1984) 769-74.